Modeling and performance analysis for masks in coded mask infrared imaging

Zhang Ao[1], Wang Qing[1], Yang Jingyu[1], Sun Yi[2]

(1. School of Electronic Information Engineering, Tianjin University, Tianjin 300072, China;
2. Tianjin Jinhang Institute of Technology Physics, Tianjin 300308, China)

Abstract: The model for infrared coded mask imaging systems was presented. It was composed with two functional components, the coded mask imaging with ideal focused lenses and the imperfection of practical lenses. The system′s point spread function (PSF) can then be represented by the diffraction pattern of the mask and the PSF of the practical lenses. The imaging results with inclined plane waves were also analyzed to achieve the variation of PSF within the view field. According to indices for mask pattern evaluation and system′s PSF assessment, mask pattern we proposed based on Dammann grating had a balanced performance for direct imaging and imaging reconstruction. Experiment shows that mask pattern for direct imaging should have more random structures, while more periodic structures in system with image reconstruction.

Key words: coded mask; infrared imaging; modeling; point spread function; Dammann grating
CLC number: TN21 **Document code:** A **Article ID:** 1007-2276(2015)10-2891-09

编码掩模红外成像的建模与性能分析

张 傲[1],汪 清[1],杨敬钰[1],孙 懿[2]

(1. 天津大学 电子信息工程学院,天津 300072; 2. 天津津航技术物理研究所,天津 300308)

摘 要: 针对编码掩模红外成像系统提出了一种建模方法。该模型将成像系统视为由两个功能部分组成，一部分为编码掩模与理想聚焦透镜的理想成像，另一部分为实际透镜自身的非理想成像。据此,系统点扩散函数可以由掩模结构的衍射模式和实际透镜的点扩散函数联合表示。此外,文中对视场内倾斜入射平面波的成像结果进行分析,从而得到了视场内的点扩散函数的变动情况。由码型及相应点扩散函数的指标评价结果可以看出,文中提出的基于 Dammann 阵列的码型结构对直接成像和图像还原处理具有较为平衡的性能。实验表明,对于编码掩模直接成像系统的码型中应当具有较多的随机性结构,而对于能够做进一步图像还原处理的系统码型中应当具有较多的周期性结构。

关键词: 编码掩模; 红外成像; 建模; 点扩散函数; Dammann 光栅

收稿日期:2015-02-07; **修订日期**:2015-03-15

基金项目:国家自然科学基金(61101223);教育部博士基金(20110032120087)

作者简介:张傲(1988-),男,硕士生,主要从事成像系统与微波信道的研究与建模。Email:zhangao@tju.edu.cn

导师简介:汪清(1982-),女,副教授,主要从事无线通信、电波传播、被动雷达方面的研究。Email:wangq@tju.edu.cn

0 Introduction

The application of coded mask in infrared imaging was first discussed by both Stephen R. Gottesman[1] and the QinetiQ Company[2]. The ideas were based on characteristics of early coded aperture imaging (in heavy ray and visible light), like wide field of view (FOV) and large field of depth focus, to help improving the quality of infrared imaging. Gottesman proposed his design succeed with the conventional coded aperture in heavy ray imaging[3], which the detected images were geometric projections of the source point light pre-coded by the mask pattern. Therefore, the diffraction of infrared with longer wavelength was not considered in the initial design, but was included into his following works to estimate systems′ imaging resolution[4-6]. The QinetiQ Company was inspired by compound eye systems in biology and hence regarded the coded aperture imaging as a system of multi-pinhole imaging with recovery algorithms of image fusion. Diffraction effects were analyzed at the beginning of their system design stage. The diffraction led to energy dispersion of the information, which meant there is a tradeoff between the convenience of measurement with more sensing cells and the algorithmic complexity for imaging reconstruction with high quality[7]. Their following works would be mainly focused on PSF control (including mask pattern design[8] and microshutter array technology[9]) and imaging reconstruction based on PSF calibration[10-11]. Recently, the compressed sensing is introduced into infrared imaging to achieve super-resolution. The sparse sampled results on focal plane are also affected by the diffraction of infrared through the coding mask[12-15].

From applications mentioned above, we can see that the study of PSF is still critical to analyze coded mask imaging. It is essential to build a complete model to simulate the PSF of the infrared imaging systems composed of coded mask and lenses. A set of criterions for PSF are also required to evaluate the mask pattern and the image reconstruction process. In this paper, the coded aperture infrared imaging system is regarded as lenses with a coded mask in front of them. The methods for infrared imaging system modeling are analyzed and the PSF within the view field is calculated. The PSF will then be examined in a set of criterions for direct imaging and imaging reconstruction. The Dammann grating is introduced into mask pattern design to get better auto-correlation properties for reconstruction. Some advises on mask design will be given according to experiment results in conclusion.

1 Modeling for coded mask infrared imaging systems

1.1 Wavefront coding with lenses

For longer wavelength, lights from distant objects can be focused by lenses. System in that circumstance can add lenses behind the mask for direct imaging (as shown in Fig.1). As the wavelength is comparable to the cell seize of mask, infrared light will result in distinct diffraction effects, i.e. the diffraction pattern, when passing through the mask. Besides, lenses, together with diaphragms, will add imperfect phase modulation to angular spectrum, defocusing the lights reached onto the focal plane. Both the defocus and diffraction effects introduce additional information and blurring for imaging results, decreasing the resolutions of direct imaging. Therefore, corresponding algorithms are needed for the image reconstruction.

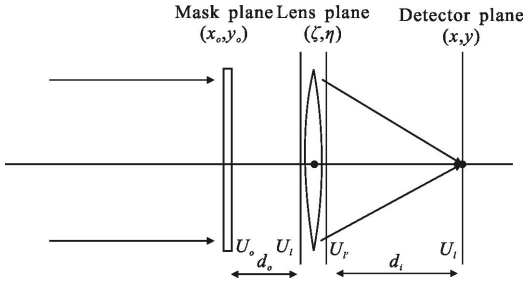

Fig.1 Coded aperture imaging systems with lenses

If the recorded image is represented by $g(x,y)$ and the original scene by $g_o(x_o,y_o)$, the image degradation

can be handled by[16]:

$$g(x,y)=h(x,y)*g_o(x_o,y_o)+n(x,y) \tag{1}$$

where * is the correlation operator. The system function is described in h and mainly influenced by mask diffraction and the defocus of lenses.

If the mask pattern is $t(x_o,y_o)$, the light field behind the mask can be represented by $u_s \cdot t(x_o,y_o)$. If the pupil is $P(\zeta,\eta)$, the transmission function of lens can be represented by:

$$t_l(\zeta,\eta)=P(\zeta,\eta)\cdot\exp\left[-j\frac{k}{2f}(\zeta^2,\eta^2)\right] \tag{2}$$

where f is the focus length and k is the wave number. Suppose λ is the wavelength.

From Fresnel diffraction theory, the amplitude distribution on the detector plane is:

$$U_i(x,y)=\frac{1}{\lambda^2 d_o d_i}\cdot\exp\left[j\frac{k}{2d_i}(x^2+y^2)\right]\times\iint\iint U_o(x_o,y_o)\cdot$$
$$\exp\left[-j\frac{2\pi}{\lambda d_o}(x_o\zeta+y_o\eta)\right]\times P(\zeta,\eta)\cdot\exp\left[-j\frac{2\pi}{\lambda d_i}(x\zeta+y\eta)\right]\times$$
$$\exp\left[j\frac{k}{2}\left(\frac{1}{d_o}+\frac{1}{d_i}-\frac{1}{f}\right)(\zeta^2,\eta^2)\right]\times\exp\left[j\frac{k}{2d_o}(x_o^2,y_o^2)\right]\cdot$$
$$\mathrm{d}\zeta\mathrm{d}\eta\cdot\mathrm{d}x_o\mathrm{d}y_o \tag{3}$$

Suppose the distance between mask and lens is very close, then we have:

$$\frac{1}{d_o}+\frac{1}{d_i}-\frac{1}{f}\approx\frac{1}{d_o} \tag{4}$$

The phase factor in the amplitude distribution is negligible, then U_i can be rewritten in:

$$U_i(x,y)=\frac{1}{\lambda^2 d_o d_i}\times\iint\{\iint U_o(x_o,y_o)$$
$$\exp\left[j\frac{k}{2d_o}(x_o^2,y_o^2)\right]\times\exp\left[-j\frac{2\pi}{\lambda d_o}(x_o\zeta+y_o\eta)\right]\mathrm{d}x_o\mathrm{d}y_o\}\times$$
$$P(\zeta,\eta)\exp\left[j\frac{k}{2d_o}(\zeta^2+\eta^2)\right]\times\exp\left[-j\frac{2\pi}{\lambda d_i}(x\zeta+y\eta)\right]\mathrm{d}\zeta\mathrm{d}\eta \tag{5}$$

Take phase factor $\exp\left[-j\frac{2\pi}{\lambda d_o}(x_o\zeta+y_o\eta)\right]$ as the basis of space transformation. Eq. (5) means that original scene is transformed into Fourier domain and back. The frequency of original scene is cut by lens′ aperture. Introducing $M=\frac{d_i}{d_o}$, Eq.(5) in unified coordinate system can be represented in:

$$U_i(x,y)=M^2\left\{U_o\left(\frac{x}{M},\frac{y}{M}\right)\exp\left[j\frac{k}{2d_o}\left(\left(\frac{x}{M}\right)^2,\left(\frac{y}{M}\right)^2\right)\right]\right\}*$$
$$F\left\{P(x,y)\exp\left[j\frac{k}{2d_o}(x^2+y^2)\right]\right\} \tag{6}$$

Eq.(6) shows that coded mask imaging system is composed of two functional structures, the coded mask imaging with ideal focused lenses and the imperfection of practical lenses, which can be shown in Fig. 2.

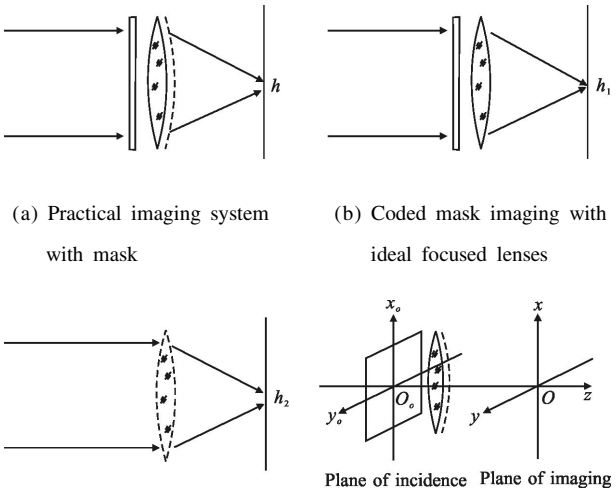

(a) Practical imaging system with mask

(b) Coded mask imaging with ideal focused lenses

(c) Imperfection of practical lenses

(d) Coordinate system to analyze systems

Fig.2 Functional composition of practical coded aperture imaging system

1.2 Imaging with normal incidence plane waves

For solely mask irradiated by plane waves with zero incident angles, the detected image is the light intensity distribution through the multi-hole mask, which is determined by Fresnel diffraction. If the mask is close followed by ideal focused lenses, imaging result on the focal plane is Fraunhofer diffraction[17]:

$$h_1(x,y)=|F\{t(x_o,y_o)\}|^2 \tag{7}$$

Where $h_1(x,y)$ is the imaging result on the focal plane for plane waves, i.e. the PSF of coded mask with ideally focused lenses.

In practical imaging system composed of mask and lenses close followed, the imperfection of lenses lead to scattering and distortion on the focal plane, which can be exactly described by the lenses′ PSF. The imperfection of lenses in our model can be noted as:

$$h_2(x,y)=f_l(x,y) \tag{8}$$

Where $f_l(x,y)$ is the lenses′ PSF.

From Eq. (5), the system function can also be represented by PSF composed with two functional components:

$$h(x,y)=h_1(x,y)*h_2(x,y)=|F\{t(x,y)\}|^2*f_l(x,y) \tag{9}$$

That means the intense pulsed light response to coded mask imaging system can be expressed by the convolution of the ideal Fraunhofer diffraction pattern of the mask and the PSF of the practical lenses with imperfection.

1.3 Imaging with inclined incident planewaves

As the coded mask imaging systems has a wide view field, the system′s PSF varies according to the inclined angle of the incident light. Equations acquired above should be modified with incident factors γ and δ, which are inclined angles to the x_o axis and y_o axis shown in Fig.3. Then Eq.(9) above gives to:

$$h(x,y;\gamma,\delta)=h_1(x_o,y_o;\gamma,\delta)*h_2(x,y;\gamma,\delta)=$$
$$|F\{t(x_o,y_o;\gamma,\delta)\}|^2*f_l(x,y;\gamma,\delta) \tag{10}$$

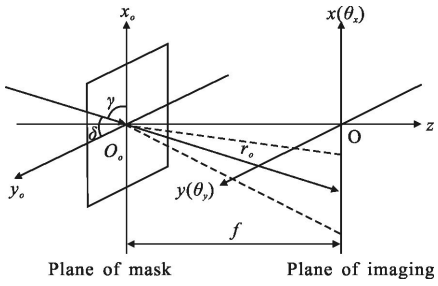

Fig.3 Mask diffraction with inclined plane waves

Lenses can be modeled in the simulation software according to their optical structures and material parameters. By varying incident angles during the simulation, PSF within the total view field, i.e. the $f_l(x,y;\gamma,\delta)$, can be achieved in the simulation outputs.

The Fraunhofer diffraction result of designed mask pattern illuminated with plane waves can be computed in Matlab. The diffraction result with zero incident angles is the square of Fourier transformation of mask pattern. But for inclined incident plane waves, the expressions also need to be modified.

When illuminated by plane waves with angles, the amplitude distribution on mask plane is:

$$U_o(x_o,y_o)=u_o\cdot\exp[-ik(x_o\cdot\cos\gamma+y_o\cdot\cos\delta)] \tag{11}$$

where u_o is the amplitude of plane waves. The exponential part in the expression is the additional phase shift introduced by incident inclination, where the optical path difference is:

$$\Delta r=-(x_o\cdot\cos\gamma+y_o\cdot\cos\delta) \tag{12}$$

After being modulated by mask, the amplitude of waves becomes $U_o(x_o,y_o)\cdot t(x_o,y_o)$. When arrived at focal plane, the complex amplitude distribution can be represented in[18]:

$$U(\theta_x,\theta_y)=\frac{-i}{\lambda f}e^{ikr_o}\iint U_o(x_o,y_o)\cdot t(x_o,y_o)\times$$
$$\exp[-ik(x_o\cdot\sin\theta_x+y_o\cdot\sin\theta_y)]\mathrm{d}x_o\mathrm{d}y_o \tag{13}$$

Where θ_x and θ_y are diffraction angles.

Take Eq.(11) into Eq.(13), then we have:

$$U(\theta_x,\theta_y)=\frac{-i}{\lambda f}e^{ikr_o}\iint u_o\cdot t(x_o,y_o)\times$$
$$\exp\{-ik[x_o(\cos\gamma+\sin\theta_x)+y_o(\cos\delta+\sin\theta_y)]\}\mathrm{d}x_o\mathrm{d}y_o \tag{14}$$

The exponential part indicates that amplitude distribution on imaging plane is a Fourier transformation projection from (x_o,y_o) plane to $(\cos\gamma+\sin\theta_x,\cos\delta+\sin\theta_y)$plane. According to definition of $x_oO_oy_o$ and xOy coordinate systems and the relative spatial position of the mask, the diffraction angle can be expressed in:

$$\sin\theta_x=\frac{x}{\sqrt{x^2+y^2+f^2}}\quad\sin\theta_y=\frac{y}{\sqrt{x^2+y^2+f^2}} \tag{15}$$

Then Eq.(14) can be rewritten as:

$$U\left(\cos\gamma+\frac{x}{\sqrt{x^2+y^2+f^2}},\cos\delta+\frac{y}{\sqrt{x^2+y^2+f^2}}\right)=$$
$$\frac{-iu_o}{\lambda f}e^{ikr_o}\cdot F\{t(x_o,y_o)\} \tag{16}$$

Which is the amplitude distribution on imaging plane with inclined incident plane waves. The corresponding intensity distribution $h_1(x_o,y_o;\gamma,\delta)$ can be expressed in:

$$h_1(x_o,y_o;\gamma,\delta)=|U(x,y;\gamma,\delta)|^2 \tag{17}$$

and the intense pulsed light response $h(x,y;\gamma,\delta)$ of coded mask system can then be represented in:

$$h(x,y;\gamma,\delta)=h_1(x_o,y_o;\gamma,\delta)*h_2(x,y;\gamma,\delta)=|U(x,y;\gamma,\delta)|^2*$$
$$f_l(x,y;\gamma,\delta) \tag{18}$$

2 Effects and evaluations of masks

For coded mask imaging with a given optical system, the mask pattern should fit for the imaging reconstruction and processing methods. There are varieties of mask patterns for different use, such as MURA[19] and DFZP[20] for heavy ray imaging, Levin pattern[21] and Zhou pattern[22-23] for depth estimation and deblurring, and random masks for compressive sensing[24-27].

2.1 Analysis for mask pattern

If a coded mask system is used for direct imaging, the optimized mask should decline the PSF′s diffusion and gather energy to PSF′s major lobe as much as possible, which guarantee the focused imaging without blur and aliasing on detector. Experiments show that mask with random holes, like Fig.4(a), will give out better angular resolution for a given SNR, because the auto-correlation of the diffraction pattern has smaller side lobes[4].

Applications fields of coded mask are expanded by digital imaging restoration techniques. The aim of using masks in imaging system with restoration is to acquire as much information about the original scene as possible[28], or to get compressed information. Information about original scene is coded when passing through the mask, and the modulation is controlled by the mask pattern. Diffraction effects are also involved into the modulation result. The detected images are no longer precisely the original scene, because the mask changes the energy distribution of the original information. Corresponding restoration algorithms are needed for information retrieval and image reconstruction with high resolution. In Levin′s work[21], the proposed mask pattern, shown in Fig.4(b), is fit for depth estimation, because it gets a high KL divergence score and the system′s PSF varies notably to source point in different depth.

Mask pattern in compressive coded mask imaging is the measurement matrix in compressive sensing theories. It has been proved that if the measurement matrix is a Gaussian random matrix, the sensing matrix can meet the restricted isometry property (RIP) in all probability and the original scene can be successfully reconstructed [12]. Lots of works on compressive imaging[12,26-29] are based on random mask pattern.

In our practical infrared imaging system, the lenses are available for wavelengths centered at 8 μm and the focus length is 84 mm. In order to acquire high resolution imaging and depth estimation, a new type of mask pattern is designed based on Dammann grating. The mask pattern, shown in Fig.4(c) as a 5×5 Dammann grating array, is still binary phase grating, but the diffraction result has sharp autocorrelation peaks and the energy is concentrated in several dots apart. It makes energy detection easier and decreases measurement error[30]. Besides, the peculiar diffraction pattern can be easily recognized because it varies according to the depth or rotation of the original scene, which helps in image reconstruction and depth estimation.

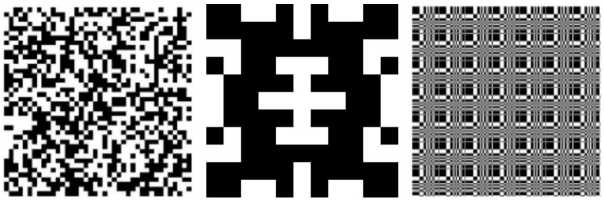

(a) 40×40 Random (b) 11×11 Levin (c) 5×5 Dammann grating

Fig.4 Different mask patterns

2.2 Criterion for coded mask imaging system

In order to evaluate the performance of designed mask pattern and the whole imaging systems, a set of indices are devised based on PSF properties related to imaging recovery. The M1 and M2 metrics are used to describe the energy percentage within a circle of radius r centered at main lobe and to assess the PSF variation within field angle[31]. Both indices determine the resolution of direct imaging. They are originally designed for lenses assessment, but introduced here to evaluate the PSF of the coded mask imaging system. The M1 and M2 are defined in:

$$M1(r)=\frac{\sum_{x,y} h(x^2+y^2+r^2)}{\sum_{x,y} h(x+y)} \tag{19}$$

$$M2(\varphi)=\frac{\sum_{x,y} h(x,y;\varphi)-h(x,y;\varphi+\Delta\varphi)}{\sum_{x,y} h(x,y;\varphi)} \tag{20}$$

where r is radius of the circle centered at the position of the chief ray and φ is the incident angel of the source point.

In procedure of high resolution reconstruction, corresponding indices are need. If a reconstruction involves filtering, the minimum resolution angle is determined by the auto-correlation of PSF. As the imaging system is always rolling during practical imaging stage, a rotation auto-correlation index RA is defined in Eq.(21) to assess the image resolution with rotational motion, where is rotation angle between image frames. Considering image depth estimation and deblurring based on Wiener deconvolution, the KL divergence[21] and $R(K)$[22] are defined for the mask selection.

$$RA(\omega)=\mathrm{corr}(h(x,y;\omega),h(x,y;\omega+\Delta\omega)) \tag{21}$$

3 Experiments

Considering a practical imaging system, where the focus length of lenses is 84 mm and the diaphragm diameter is 10.65 mm. The illuminating wavelengths are centered at 8 μm. The PSF of the lenses can be acquired from lenses′ data sheet and it′s shown in linear in Fig.5.

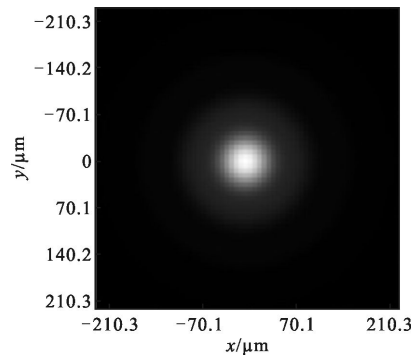

Fig.5 PSF of imaging lenses

3.1 Experimental results with masks

Experiments focus on five mask patterns: random patterns with 200 ×200 and 1 000 ×1 000 coding matrixes, the Levin pattern and Dammann grating patterns in 5×5 and 25×25 arrays. All the masks are designed in squares with sided length of 30 mm, and sampled by 1 200×1 200 matrixes in Matlab. The PSFs of the practical imaging systems with these five masks are shown in Fig.6.

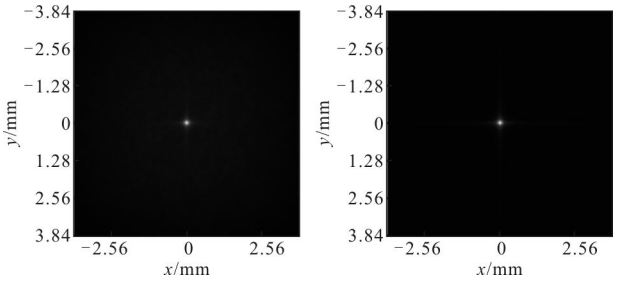

(a) 200×200 random (b) 1 000×1 000 random

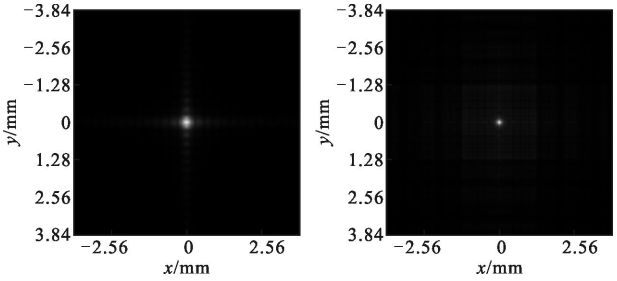

(c) Levin (d) 5×5 Dammann grating array

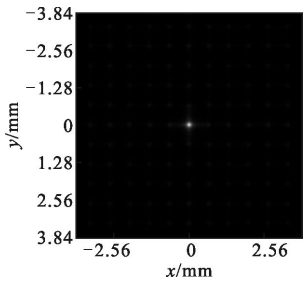

(e) 25×25 Dammann grating array

Fig.6 PSFs of the practical imaging systems with different masks

If illuminated by inclination incident plane waves within the view field, the system′s corresponding diffraction patterns can be acquired from Eq. (18). Take 25×25 Dammann grating array for example, the results with inclination are shown in Fig.7.

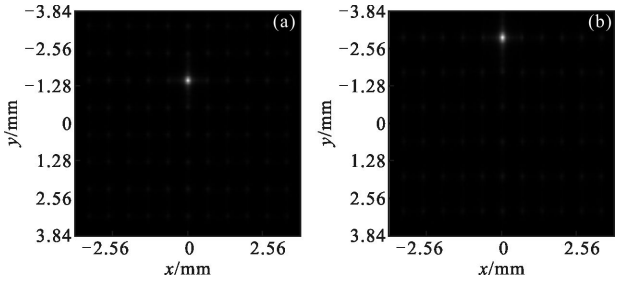

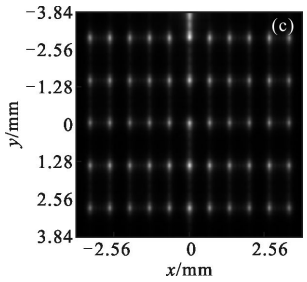

Fig.7 Diffraction results of 25*25 Dammann grating array with inclined illumination

The M1, M2 and the rotation auto-relation (RA) of each mask are shown in Fig.8.

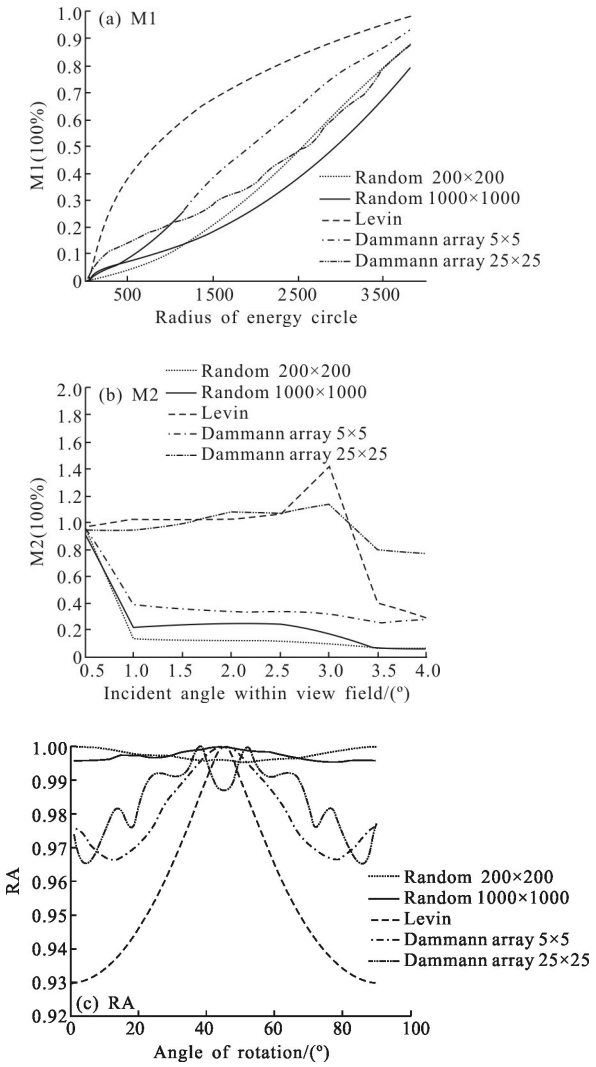

Fig.8 M1, M2 and RA results for different mask patterns

3.2 Results analysis

From the diffraction results in Fig.5 and Fig.6 we can see that, in imaging system with a mask, the main lobe energy of diffraction is stronger comparing to that in system only with lenses, but the width of main lobe is reduced relatively. Besides, the side lobe energy is concentrated and enhanced at several points, which are perceptible to detector. If masks are designed with same pattern but in smaller cell size, most of the energy will concentrated on the main lobe and the side lobes will fade out. Comparing different mask patterns, energy passing through random patterns is almost concentrated near the chief ray; while with periodic mask patterns, more energy is distributed on the region around chief ray. If mask pattern combines random and periodic structures, the energy distribution will focus on several side lobes beside the main lobe. By adjusting the combination of random and periodic arrangement, desired diffraction pattern can be achieved.

Figure 8 (a) shows that in system with random mask pattern, main lobe energy is sharply focused and the rest energy is uniformly distributed onto the whole detector. The M1 curve for random mask, therefore, is concave as the energy circle expands. The Levin pattern gathers most of the energy around the main lobe, resulting in a convex curve in M1 chart. Curves of Dammann patterns are between these two sorts, and they are not smooth because of the existence of additional energy dots.

The variances of PSF with inclinations can be analyzed from Fig.8(b). Random pattern gets a quick descent when incident waves are inclined with small angles, which means the PSF alters greatly around the primary optical axis. The Levin pattern has a gentle curve with higher amplitude, which means the variance of PSF can be easily detected. Dammann pattern has a balanced combination of these two sorts of characters.

Seeing from Fig.8(c), system with random pattern is not sensitive to rotation, while sensitive when using Levin pattern, which is periodical and symmetric. Dammann pattern is sensitive at several rotation angles.

There is a loss in energy if the coded mask is

inserted in the optical path, because the mask is partially occupied by blocks and the diffraction disperses some energy under the threshold of sensing cells. Besides, the thermal noise will be inevitability increased due to the mask materials. Both effects will decrease SNR detected. But the decoding process with a prior information of mask modulation will bring about coding gain.

4 Conclusions

This paper describes a modeling method for infrared imaging system with coded mask placed in front of lenses. The imaging result for plane waves is decided by the mask pattern and the imperfection of lenses, so the system is modeled as tow parts: mask with ideally focused lenses and practical lenses with imperfection. The mask part is modeled as Fraunhofer diffraction and it will be modulated by the imperfect lenses to achieve the total PSF of the system. The variation of pattern is analyzed within the view field. A set of metrics are designed according to reconstruction methods to evaluate the PSF of whole imaging system.

Numerical experiments show that the model matches practical measurement. For direct imaging system with coded mask, the mask pattern should be close to random distribution and the cell size should be reduced. If coded mask are used in system with digital imaging processing, the PSF should vary with the source position, which means there need to be more periodic pattern in the mask and the cell size should be increased. The Dammann grating pattern has a balanced performance in the both requirements.

The built model allows to analyze the mask and lenses separately and simplify calculations. The criterions are able to assist with mask design and evaluation of the PSF. However, there are still limitations in our model. The thickness of coded mask need to be considered as the cell size becomes smaller. Besides, the aero-optical effects together with thermal noise are also inevitable in practical applications. The image resolution of infrared coded imaging system will also be discussed in our future studies.

Reference:

[1] Wakin M B, Wakin M B, Laska J N, et al. An architecture for compressive imaging [C]//2006 IEEE International Conference on Image Processing, 2006: 1273−1276.

[2] Lewis K. Challenges in the evolution of advanced imaging systems [C]//Adaptive Coded Aperture Imaging and Non-Imaging Sensors, 2007, 6714: 671402.

[3] Gottesman S R. Coded apertures: past, present, and future application and design[C]//Adaptive Coded Aperture Imaging and Non-Imaging Sensors, 2007, 6714: 671405.

[4] Gottesman S R, Shrekenhamerb A, Issera A, et al. A systematic investigation of large-scale diffractive coded aperture designs [C]//Unconventional Imaging and Wavefront Sensings, 2012, 8520: 852008.

[5] Gottesman S R, Isser A, Gigioli J G W. Adaptive coded aperture imaging: progress and potential future applications [C]//Unconventional Imaging, Wavefront Sensing, and Adaptive Coded Aperture Imaging and Non-Imaging Sensor Systems, 2011, 8165: 816513.

[6] Gottesman S R, Isser A, Gigioli J G W. Adaptive coded apertures: bridging the gap between non-diffractive and diffractive imaging systems [C]//Adaptive Coded Aperture Imaging, Non-Imaging, and Unconventional Imaging Sensor Systems II, 2010, 7818: 781805.

[7] Slinger C, De Villiers G, Wilson R, et al. An investigation of the potential for the use of a high resolution adaptive coded aperture system in the mid-wave infrared[C]//Adaptive Coded Aperture Imaging and Non-Imaging Sensors, 2007, 6714: 671408.

[8] Stayman J W, Subotic N, Buller W. An analysis of coded aperture acquisition and reconstruction using multi-frame code sequences for relaxed optical design constraints [C]// Adaptive Coded Aperture Imaging, Non-Imaging, and Unconventional Imaging Sensor Systems, 2009, 7468: 74680D.

[9] Slinger C, Wilson R, Gordon N, et al. Coded aperture systems as non-conventional lensless imagers for the visible and infrared [C]//Electro-Optical and Infrared Systems: Technology and Applications IV, 2007, 6737: 67370D.

[10] Slinger C W, Watson P, Wilson R, et al. Adaptive coded aperture imaging in the infrared towards a practical

implementation [C]//Adaptive Coded Aperture Imaging and Non-Imaging Sensors II, Proceedings of the SPIE, 2008, 7096: 709609.

[11] De Villiers G D, Gordon N T, Payne D A, et al. Sub-pixel super-resolution by decoding frames from a reconfigurable coded aperture camera: theory and experimental verification [C]//SPIE, 2009, 7468: 746806.

[12] Xiao L, Liu K, Han D, et al. A compressed sensing approach for enhancing infrared imaging resolution[J]. ***Optics & Laser Technology***, 2012, 44(8): 2354-2360.

[13] Xiao Longlong, Liu Kun, Han Dapeng, et al. Focal plane coding method for high resolution infrared imaging [J]. ***Infrared and Laser Engineering***, 2011, 40(11): 2065-2070. (in Chinese)
肖龙龙, 刘昆, 韩大鹏, 等. 焦平面编码高分辨率红外成像方法[J]. 红外与激光工程, 2011, 40(11): 2065-2070.

[14] Guo Junwei. Imaging system of synchronous sample and compression based on CS theory [J]. ***Chinese Optics and Applied Optics Abstracts***, 2010, 2(6): 525-530. (in Chinese)
郭军伟. 应用 CS 理论实现同步采样压缩成像[J]. 中国光学与应用光学, 2010, 2 (6): 525-530.

[15] Liu Jingdan, Xu Tingfa, Xun Xianchao, et al. Simulation of geometric superresolution imaging by using optical mask [J]. ***Optics and Precision Engineering***, 2014, 22(8): 2026-2031. (in Chinese)
刘晶丹, 许廷发, 荀显超, 等. 光学掩模实现几何超分辨成像的仿真[J]. 光学 精密工程, 2014, 22(8): 2026-2031.

[16] Zhuo Li, Wang Suyu, Li Xiaoguang. Image/Video Super Resolution [M]. Beijing: Posts & Telecom Press, 2011. (in Chinese)
卓力, 王素玉, 李晓光. 图像/视频的超分辨率复原[M]. 北京: 人民邮电出版社, 2011.

[17] Lv Naiguang. Fourier Optics [M]. 2ed ed. Beijing: China Machine Press, 2013. (in Chinese)
吕乃光. 傅里叶光学[M]. 2 版. 北京:机械工业出版社, 2013.

[18] Li Z, Cen Y. Diffraction field of parallel light oblique incident on rectangle hole [J]. ***Physics Experimentation***, 2011, 31(8): 43-46.

[19] Gottesman S R, Fenimore E E. New family of binary arrays for coded aperture imaging [J]. ***Appl Opt***, 1989, 28 (20): 4344-4352.

[20] Kipp L, Skibowski M, Johnson R L, et al. Sharper images by focusing soft X-rays with photon sieves [J]. ***Nature***, 2001, 414(6860): 184-188.

[21] Levin A, Fergus R, Durand F, et al. Image and depth from a conventional camera with a coded aperture [C]// Annual Conference on Computer Graphics, 2007.

[22] Changyin Z, Nayar S. What are good apertures for defocus deblurring [C]//ICCP, 2009.

[23] Zhou C, Lin S, Nayar S K. Coded Aperture Pairs for Depth from Defocus and Defocus Deblurring [J]. ***International Journal of Computer Vision***, 2011, 93(1): 53-72.

[24] Takhar D, Laska J N, Wakin M B, et al. A new compressive imaging camera architecture using optical-domain compression [C]//2006 IEEE International Conference on Image Processing, 2006, 6065: 606509.

[25] Xu X. Encoded optical compressive imaging architectures and reconstruction algorithms[D]. Xi′an: Xidian University, 2011.

[26] Marcia R F, Harmany Z T, Willett R M. Compressive coded apertures for high-resolution imaging [C]//SPIE Photonics Europe, International Society for Optics and Photonics, 2010, 7723: 772304.

[27] Marcia R F, Harmany Z T, Willett R M. Compressive coded aperture imaging [C]//IS&T/SPIE Electronic Imaging, International Society for Optics and Photonics, 2009, 7246: 72460G.

[28] Yang Xiao, Yang Xueyou, Ye Shenghua. Arbitrary shape ROI image encoding at low bit rate[J]. ***Optics and Precision Engineering***, 2012, 20(4): 896-905. (in Chinese)
杨晓, 杨学友, 叶声华. 低码率下任意形状感兴趣区域编码[J]. 光学 精密工程, 2012, 20 (4): 896-905.

[29] Stern A, Rivenson Y, Javidi B. Optically compressed image sensing using random aperture coding[C]//Enabling Photonics Technologies for Defense, Security, and Aerospace Applications IV, 2008, 6975: 69750D.

[30] Leng Yanbing, Dong Lianhe, Sun Yanjun. Study on 1×11 Dammann grating with sub-wavelength structure[J]. ***Infrared and Laser Engineering***, 2014, 43(3): 812-817. (in Chinese)
冷雁冰, 董连和, 孙艳军. 1× 11 亚波长结构 Dammann 光栅的研制[J]. 红外与激光工程, 2014, 43(3): 812-817.

[31] Bennett C R, Ridley K D, de Villiers G D, et al. Optical design of a coded aperture infrared imaging system with resolution below the pixel limit[C]//Adaptive Coded Aperture Imaging, Non-Imaging, and Unconventional Imaging Sensor Systems II, 2010, 7818: 78180H.